Electronic Supplementary Material (ESI) for Journal of Materials Chemistry A.

Supporting Information

Toward strong X-band-electromagnetic-wave-absorbing materials: Polyimide/carbon nanotubes composite aerogel with radial needle-like porous structure

Shi Liu, Qiang Xu, Yuting Bai, Xu Wang, Xiangyang Liu, Cenqi Yan, Yinghan Wang, Jiaqiang Qin*, Pei Cheng*

College of Polymer Science and Engineering, State Key Laboratory of Polymer Materials Engineering, Sichuan University, Chengdu, 610065, People's Republic of China.

*Corresponding Author(s): E-mail: jqqin@scu.edu.cn, chengpei@scu.edu.cn

Experimental

Preparation of pure PI aerogel

The PAAS powder was dissolved in deionized water, and the solid content was controlled to 5.47 wt%. Then the solution was sonicated until PAAS was completely dissolved, and the PAAS aqueous solution was obtained. The PAAS aqueous solution was then transferred to a mold with a Teflon jacket and a rubber stopper bottom, and liquid nitrogen was poured from around the mold. Ice nuclei were rapidly formed under the action of liquid nitrogen, and ice crystals would grow rapidly from around the mold toward the center due to the temperature gradient. At the same time, the PAAS were excluded between the ice crystals, forming the PAAS cell wall. Then freeze-drying in a freeze dryer (-53 ℃, 10 Pa) for 36 h to obtain PAAS aerogel. Finally, the dried PAAS aerogel was heated under vacuum conditions at temperature of 100 °C, 200 °C, 250 °C, and 400 °C for 1 h, 1 h, 1 h, and 0.5 h respectively to induce thermal imidization and obtain pure PI aerogel.

Preparation of pure CNT aerogel

13 wt% water-soluble MWCNTs slurry was added to deionized water, and the solid content of MWCNTs was controlled to 5.47 wt%. Then the dispersion was sonicated to complete dispersion of CNT. The dispersion was then transferred to a mold with a Teflon jacket and a rubber stopper bottom, and liquid nitrogen was poured from around the mold. Ice nuclei were rapidly formed under the action of liquid nitrogen, and ice crystals would grow rapidly from around the mold toward the center due to the temperature gradient. At the same time, CNT was excluded between the ice crystals, forming the CNT cell wall. Then freeze-drying in a freeze dryer (-53 ℃, 10 Pa) for 36 h to obtain pure CNT aerogel.

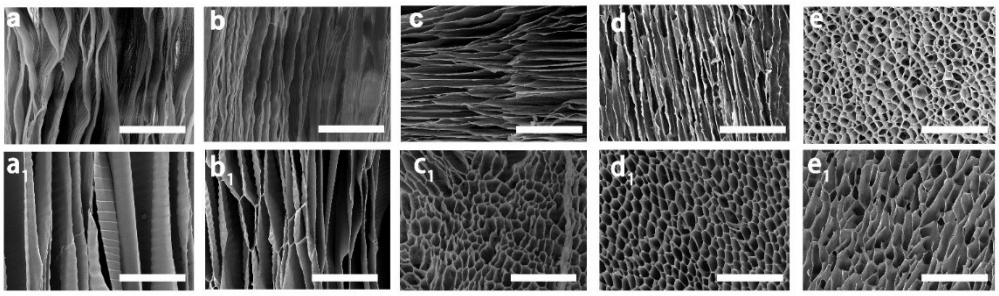

Fig. S1. Axial (a, b, c, d, e) and radial (a_1, b_1, c_1, d_1, e_1) SEM of PI aerogels prepared by radial freeze-drying with different solid content. (The solid content from left to right is 2 wt%, 2.5 wt%, 3 wt%, 3.5 wt% and 5wt%, scale = 100 μm)

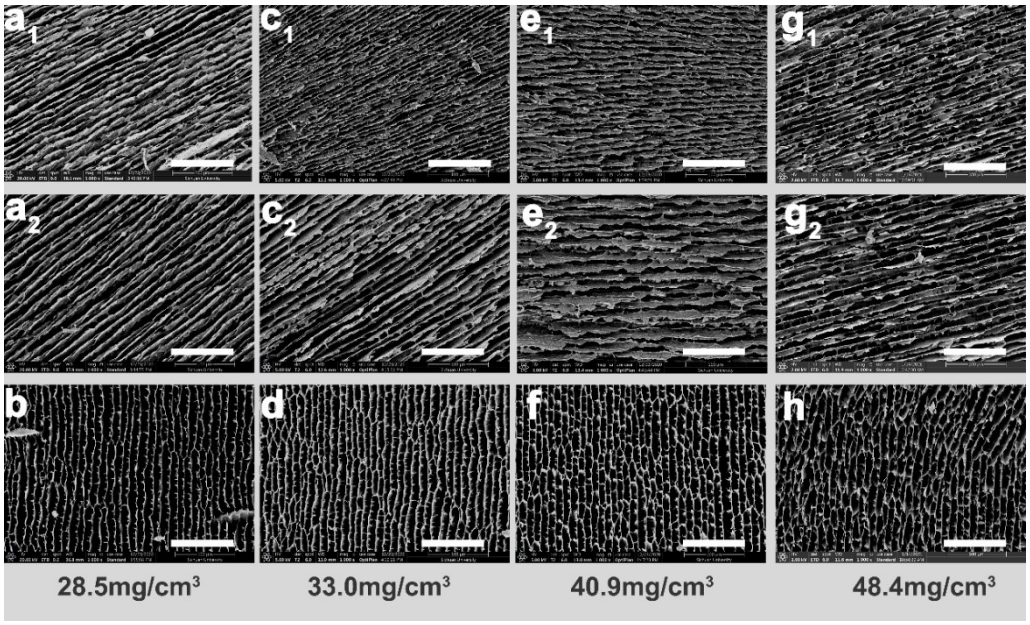

Fig. S2. Axial (a, c, e, g) and radial (b, d, f, h) SEM of O-PI/CNT (PI: CNT =1:2) aerogels with different densities (scale = 100 μm).

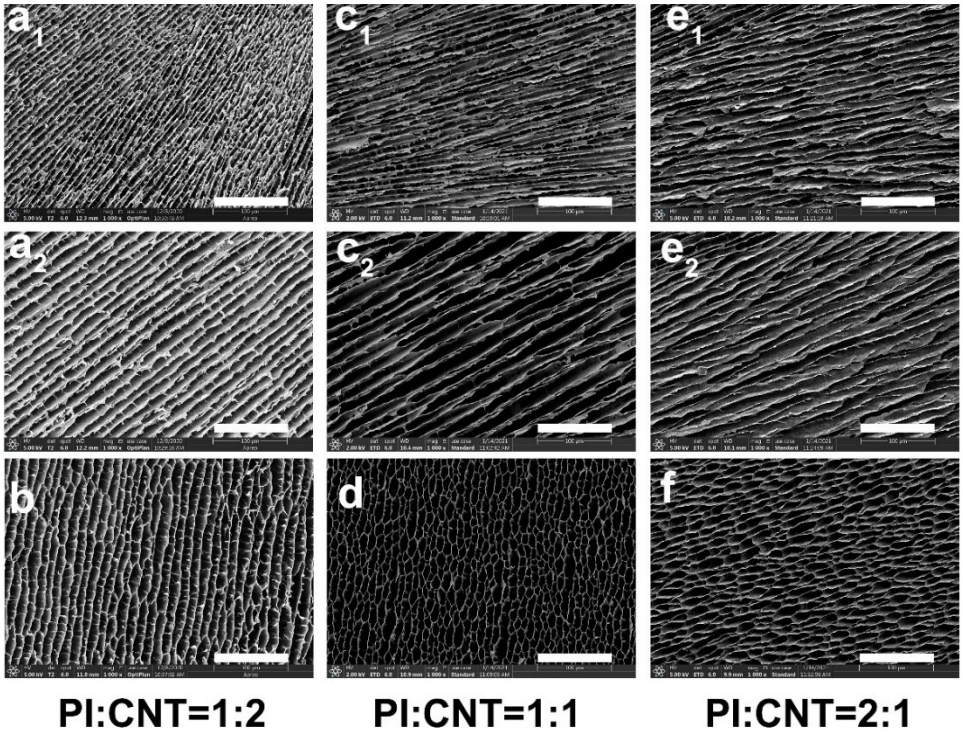

Fig. S3. Axial (a, c, e) and radial (b, d, f) SEM of O-PI/CNT (36.2 mg/cm^3) aerogels with different weight ratios of PI and CNT (scale = 100 μm).

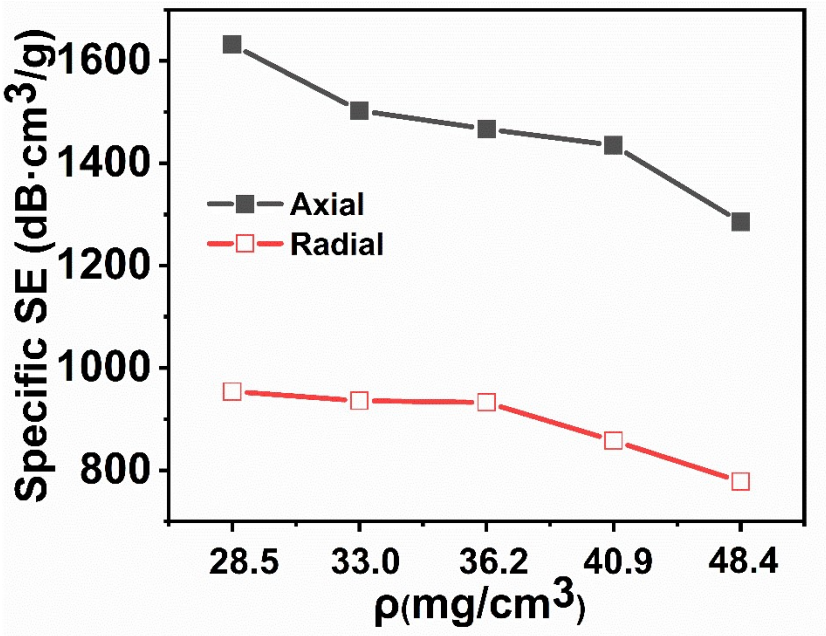

Fig. S4. Axial and radial SSE of O-PI/CNT (PI: CNT=1: 2) aerogels with different density.

Table S1

Comparison of the EMI SE and SE_A/SE_T of polymer/carbon aerogels and foam.

Materials	Thickness (mm)	EMI SE (dB)	SE_A/SE_T (%)	Ref
MXene/aramid nanofiber	2.5	65.5	83.9	1
MXene/wood-derived porous carbon	3	71.3	78.9	2
Ti_2CT_x MXene/Poly (vinyl alcohol)	5	28	92.8	3
MXene ($Ti_3C_2T_x$)/PEDOT: PSS	5	59	95	4
rGO@FeNi/Epoxy	3	46	92.3	5
MXene@Wood nanocomposite	10	72	91.6	6
Wood-Derived Porous Carbon/Ni	2	50.8	84.6	7
Epoxy/CNT	3	53.1	82.5	8
polyethylene/CNT	2.1	46.4	91.8	9
Polypropylene/CNT	2	34	81	10
Polyetherimide/ Graphene	2.3	22.5	80	11
thermoplastic polyurethaneT/CNT	2	49.4	84.6	12
thermoplastic polyurethane/CNT/Ag	2	71.4	92.1	12
polyimide/graphene	2.5	22.2	95	13
polydimethylsiloxane/CNT	2	43	82	14
O-PI/CNT-axial	2	53.1	94.5	This work
O-PI/CNT-axial	3	77.1	98.5	This work
O-PI/CNT-radial	2	33.8	92.3	This work

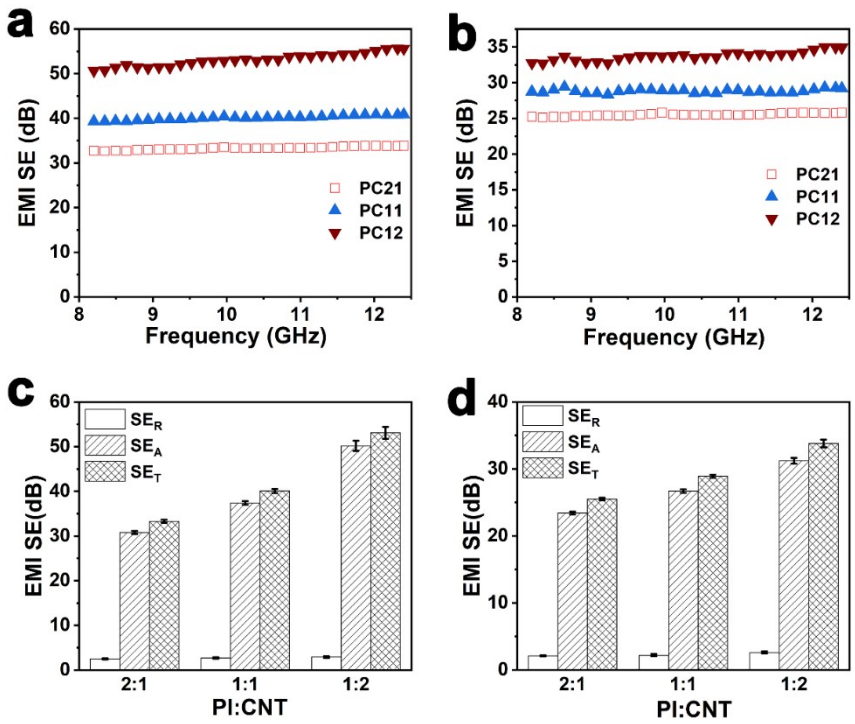

Fig. S5. Axial (a, c) and radial (b, d) EMI shielding performance of O-PI/CNT (36.2 mg/cm^3) aerogels in X-band with different weight ratios; and the comparison of SE_R, SE_A and SE_T.

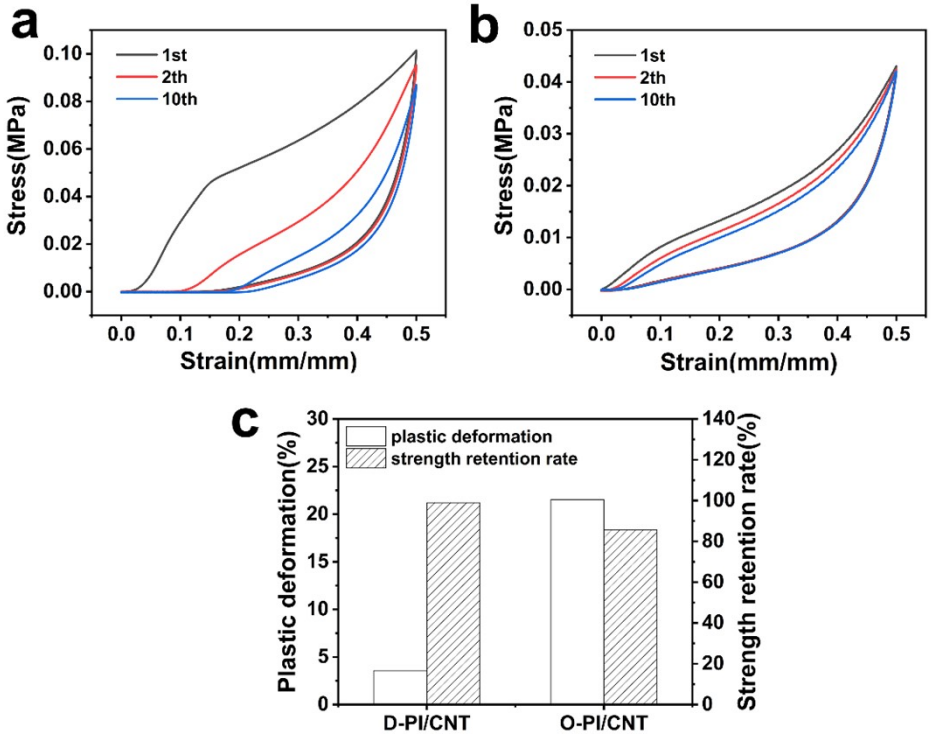

Fig. S6. Axial cyclic compression curves of D-PI/CNT (a) and O-PI/CNT. (c) the plastic deformation and compression strength retention ratio of D-PI/CNT and O-PI/CNT after 10 cycles.

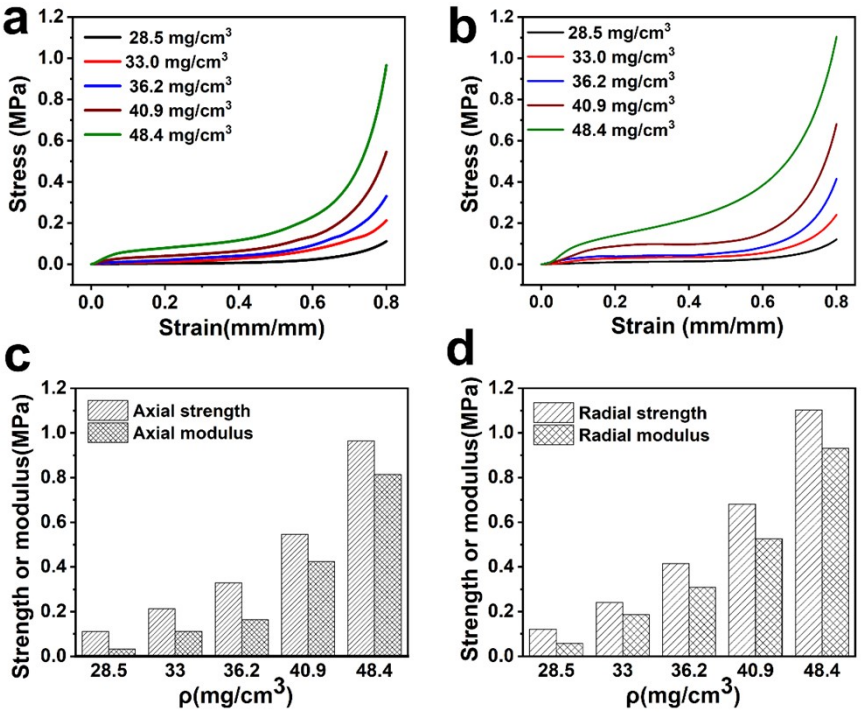

Fig. S7. Axial (a, c) and radial (b, d) compressive stress-strain curves and compressive strength, modulus of O-PI/CNT (PI: CNT=1: 2) aerogels with different densities.

References

1 Q. Gao, J. Qin, B. Guo, X. Fan, F. Wang, Y. Zhang, R. Xiao, F. Huang, X. Shi and G. Zhang, *Composites, Part A*, 2021, **151**.

2 C. Liang, H. Qiu, P. Song, X. Shi, J. Kong and J. Gu, *Sci. Bull.*, 2020, **65**, 616-622.

3 H. Xu, X. Yin, X. Li, M. Li, S. Liang, L. Zhang and L. Cheng, *ACS Appl. Mater. Interfaces*, 2019, **11**, 10198-10207.

4 G. Y. Yang, S. Z. Wang, H. T. Sun, X. M. Yao, C. B. Li, Y. J. Li and J. J. Jiang, *ACS Appl. Mater. Interfaces*, 2021, **13**, 57521-57531.

5 P. Song, Z. Ma, H. Qiu, Y. Ru and J. Gu, *Nanomicro Lett*, 2022, **14**, 51.

6 M. Zhu, X. Yan, H. Xu, Y. Xu and L. Kong, *Carbon*, 2021, **182**, 806-814.

7 Y. Zheng, Y. Song, T. Gao, S. Yan, H. Hu, F. Cao, Y. Duan and X. Zhang, *ACS Appl. Mater. Interfaces*, 2020, **12**, 40802-40814.

8 H. Mei, X. Zhao, J. Xia, F. Wei, D. Han, S. Xiao and L. Cheng, *Materials & Design*, 2018, **144**, 323-330.

9 L.-C. Jia, D.-X. Yan, C.-H. Cui, X. Jiang, X. Ji and Z.-M. Li, *J. Mater. Chem. C*, 2015, **3**, 9369-9378.

10 Y.-P. Zhang, C.-G. Zhou, W.-J. Sun, T. Wang, L.-C. Jia, D.-X. Yan and Z.-M. Li, *Compos. Sci. Technol.*, 2020, **197**.

11 J. Ling, W. Zhai, W. Feng, B. Shen, J. Zhang and W. Zheng, *ACS Appl. Mater. Interfaces*, 2013, **5**, 2677-2684.

12 B. Sun, S. Sun, P. He, H.-Y. Mi, B. Dong, C. Liu and C. Shen, *Chem. Eng. J.*, 2021, **416**, 129083.

13 Z. Yu, T. Dai, S. Yuan, H. Zou and P. Liu, *ACS Appl. Mater. Interfaces*, 2020, **12**, 30990-31001.

14 W. Xiao, X. Han, X. Niu, J. Lin, X. Han, A. He, Q. Jiang and H. Nie, *Adv. Mater. Technol.*, 2021, **6**, 2100013.